# Towards the Effect of the Fluid Ftructure Coupling on the Aeroacoustic Instabilities of Solid Rocket Motors

Julien Richard, Franck Nicoud

CSMA 2011
10e Colloque National en Calcul des Structures
9-13 Mai 2011, Presqu'île de Giens (Var)

# Towards the Effect of the Fluid Ftructure Coupling on the Aeroacoustic Instabilities of Solid Rocket Motors

J. Richard[1], F. Nicoud[2]

[1] *CERFACS, France, julien.richard@cerfacs.fr*
[2] *I3M UMR CNRS 5149, France, franck.nicoud@univ-montp2.fr*

**Résumé** — The industrial optimization needs nowadays the treatment of coupled phenomena such as aero-thermal or aero-elasticity. The following paper presents the construction and validation of a coupled software assembly, through the realization of simple test cases with a known analytical solution, with the aim to subsequently use it to solve an industrial configuration coming from the solid propulsion.
**Mots clés** — Fluid-structure interaction, unstationary, LES.

## 1 Introduction

Large solid propellant rocket motors may suffer aero-acoustic instabilities arising from a coupling between the burnt gas flow and the acoustic eigenmodes of the combustion chamber [3]. During the firing, these instabilities generate pressure oscillations leading to thrust oscillations that could endanger the launcher integrity. Given the size and cost of any single firing test or launch, being able to predict and avoid these instabilities at the design level is of the utmost industrial importance. The full scale calculations of the Ariane 5 Solid Rocket Motors (P230) have allowed to highlight the impact of fluid-structure coupling on some elements of the structure such as the frontal thermal inhibitors. Inhibitors are designed with elastomers which burn at a lower speed than propergol, creating diaphragms with small rigidity across the flow. The large deformation and the flapping of these thermal inhibitors have already been calculated in a fully coupled way in the region of the second segment [19] . It was shown that they have a strong influence on the amplitude of the thrust oscillations [15][4] . However, interaction between the structural response of some parts of the launcher, like the head end or the propergol, with the instabilities have not been investigated. The objective of this paper is to evaluate and validate the articulation of the numerical tools needed for these investigations, through the realization of simple test cases for which analytical solution can be obtained. This will lead, in a latter paper to an application on a subscaled version of the Ariane 5 SRM.

## 2 Presentation of the numerical software

Classically, the fluid-structure interaction problem consits in solving simultaneously both the fluid (1) and the structural (2) equations where some variables of one work as a source term for the other.

$$\frac{d}{dt}(AW) + F^c(W,\vec{x},\dot{\vec{x}}) = R(W,\vec{x}) \tag{1}$$

$$M\frac{d^2}{dt}(\vec{U}) + D\frac{d}{dt}(\vec{U}) + K\vec{U} = f^{ext}(W(\vec{x},t),\vec{x}) \tag{2}$$

In this semidiscrete formulation already presented by Lesoinne in [10], dots stand for time-derivatives, $\vec{x}$ is the displacement or position vector of the moving fluid grid points, W is the fluid state vector, A results from the discretization of the fluid equations, $F^c = F - \dot{x}W$ is the vector of Arbitrary Lagrangian Eulerian (ALE) convective fluxes, F is the vector of convective fluxes, R the vector of diffusive fluxes, $\vec{U}$ the structural displacement vector, and finally M, D and K are respectively the mass, damping and stiffness matrices of the structural system. In order to solve the problem of fluid-structure interactions, we have chosen to use a Conventional Serial Staggered (CSS) method with subcycling, which has already

been well studied and advocated [6][13][14]. Used software are quicly presented in this part, then the CSS method is reminded.

## 2.1 AVBP

Two different modeling tools are used for this work. First of all, aero-acoustics calculations are performed with the Large Eddy Simulation (LES) solver AVBP [17] developed at CERFACS and IFP, which has already been validated for aero-acoustic applications [16] . AVBP is designed to solve the Navier-Stokes equations for three-dimensional compressible flows over unstructured meshes. The numerical discretization can be based on a Lax-Wendroff scheme which is 2nd order in both space and time. The sub-grid scale terms are modelled thanks to the Smagorinsky or the WALE model [12].

## 2.2 MARC

The solids deformations are computed thanks to the structural analysis software MARC, using a finite element method (FEM) and developed by MSC-SOFTWARE. It is specialized in the treatment of non-linear materials, commonly encountered in solid propulsion. It allows static, dynamic and modal computations [20]. The numerical scheme used in our computations is the trapezoidal Newmark method [8] which has already been advocated for coupling applications [7][14]. It consists of writing the structure's equilibrium at the time $t^{n+1}$, knowing its state at $t^n$, and the external force $f$ at $t^{n+1}$ :

$$\left(\frac{4}{\Delta t_s^2}M+\frac{2}{\Delta t_s}D+K\right)u^{n+1}=f^{n+1}+\left(\frac{4}{\Delta t_s^2}M+\frac{2}{\Delta t_s}D\right)u^n+\left(\frac{4}{\Delta t_s}M+D\right)\dot{u}^n+M\ddot{u}^n \tag{3}$$

## 2.3 PALM

The PALM coupler developed at CERFACS is used to synchronize these two solvers [2]. It also provides data transmission between the different tools at the fluid-structure interface without large intrusion in the different solvers. As a first step, the interpolation between the unmatching meshes is achieved with a nearest-point method.

## 2.4 Coupling architecture

In most cases the time step $\Delta t_f$ for the fluid is smaller than the structural one $\Delta t_s$. We consider that the coupling time step $\Delta t_c$ is equal to the structural one $\Delta t_s$. The following steps are done for each coupling step of the CSS method in order to go from $t^n$ to $t^{n+1}=t^n+\Delta t_s$ :

- 1 : Predict the structural $u^{n+1\,p}$ displacement at time $t^{n+1}$. A common predictor is :

$$u^{n+1\,p}=u^n+\alpha_0\Delta t_s\dot{u}^n+\alpha_1\Delta t_s(\dot{u}^n-\dot{u}^{n-1}) \tag{4}$$

  It is worth to notice that the choice of $\alpha_0=1$ and $\alpha_1=0$ raises to a first order predictor, while $\alpha_0=1$ and $\alpha_1=0.5$ defines a second order predictor.
- 2 : Advance the fluid system to $t^n+\Delta t_s$ while updating the position of the fluid grid in order to match the position $u^{n+1\,p}$ at the end of the coupling steps. Because $\Delta t_f<\Delta t_s$ this step is achieve by subcycling the fluid solver.
- 3 : Transfer the fluid pressure $P_S^{n+1}$ to the structure. It's worth to notice that $P_S^{n+1}$ is not necessary the fluid pressure at the interface at time $t^{n+1}$. Many choices for $P_S^{n+1}$ can be found in the literature and we have retained three of them which are explained in details later.
- 4 : Finally integrate the structure to $t^{n+1}$.

In order to ensure the Geometric Conservation Law (GCL) [11] the velocity of the fluid/structure interface is kept constant during the subcycling and equal to $\frac{u^{n+1\,p}-u^{n\,p}}{\Delta t_s}$ . If no thermal inhibitors are considered, the assumption of small deformations is well justified in the context of solid propulsion described in the introduction. This approximation allows to model the wall motion in the LES solver by a transpiration boundary condition, which reproduces correctly the coupled solid surfaces motion speed [13][18]. This approach was preferred as a first step since it avoids considering mesh deformation, so it simplifies the overall chain complexity.

# 3 0D test configuration

## 3.1 Device description

The coupled system is composed for its fluid portion of an adiabatic room, closed at its left side by a fixed wall and at its right by a movable piston. It has a section $S_0$ and a length $L_0$ when the piston is at $x = 0$. The piston has a mass m and is attached to an external fixed point through a spring of rigidity k. Displacement, velocity, and acceleration of the piston at time $t$ are respectively $x(t)$, $\dot{x}(t)$, and $\ddot{x}(t)$.

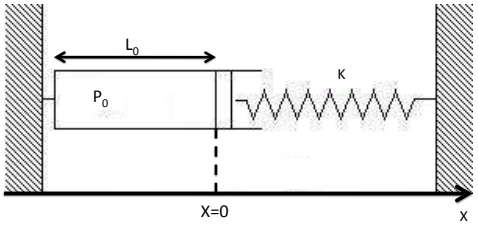


The following assumptions are first made for the system :
- The gas is perfect with an adiabatic coefficient $\gamma$
- The gravity effect is neglected
- The spring mass is neglected
- The spring is considered with no dissipation

FIGURE 1 – 0D coupling system

## 3.2 0D Modelling

Lefrançois and Boufflet have shown in [9] that applying Newton's second law to the piston and considering that its position at rest corresponds to $x(t) = \dot{x(t)} = \ddot{x(t)} = 0$ and $P = P_0$ leads to :

$$m\ddot{x}(t) = -k\,x(t) + S_0\,(P(x(t),t) - P_0) \tag{5}$$

All fluid variables are supposed to be to be uniform in the chamber (0D assumption), which means that $P(x(t),t) = P(t)$. Due to adiabatic walls, there is no thermal flux between the gas and the chamber. Then, supposing that the compression is done in reversible way, allows to apply Laplace's law which states that :

$$P(x(t),t) = P(t) = \frac{P_0\,L_0^{\gamma}}{(L_0 + x(t))^{\gamma}} \tag{6}$$

By re-injecting (6) in (5) and linearizing for small displacements around x = 0, we get :

$$m * \ddot{x}(t) = -k\,x(t) + S_0\,\frac{-\gamma\,P_0}{L_0}\,x(t) \tag{7}$$

Solving (7) gives us both the temporal evolution of the piston position and the chamber's pressure. This corresponds respectively to equations (8) and (9).

$$x(t) = x_0\,\cos\left(\sqrt{\frac{k + \gamma P_0 S_0/L_0}{m}}\,t\right) \tag{8}$$

$$P(t) = P_0 + \frac{\gamma P_0}{L_0} x_0 \cos\left(\sqrt{\frac{k + \gamma P_0 S_0/L_0}{m}}\,t + \pi\right) = P_0 + P_1 \cos\left(\sqrt{\frac{k + \gamma P_0 S_0/L_0}{m}}\,t + \pi\right) \tag{9}$$

## 3.3 Energy consideration

By using a simple switch of variable, it is possible to write that pressure and structure are vibrating at the same circular frequency $\omega = \sqrt{\frac{k+\gamma P_0 S_0/L_0}{m}}$, but with a phase difference $\phi = \pi$.
Two scalars are introduced as follow : $k_e = x_0\,P_1 \cos(\phi)$, and $h = \omega \Delta t_c$. Piperno and Fahrat [14] have

calculated the amount of energy imbalance created at the fluid structure interface $\Delta E_N$ after $N$ oscillations for a general case including structural dissipation and for different choices of $P_S^{n+1}$ . According to their results $\Delta E_N \sim N\pi(\delta E_F + \delta E_S)$ and in our particular case with subcycling we have :

$$\delta E_F = k_e \left[ (\alpha_0 - 1)h + \left( \frac{1}{4} - \frac{7\alpha_0}{12} + \frac{3\alpha_1}{2} \right) h^3 \right] + O(h^4) \tag{10}$$

$\delta E_S$ is depending on the choice of $P_S^{n+1}$.
For the first choice, $P_S^{n+1} = P^{n+1}$ :

$$\delta E_S = O(h^4) \tag{11}$$

For the second choice, $P_S^{n+1} = \frac{1}{\Delta t_c} \int_{t^n}^{t^{n+1}} P(t)dt$ :

$$\delta E_S = k_e \left[ -\frac{h}{2} + \frac{h^3}{8} \right] + O(h^4) \tag{12}$$

For the third choice, $P_S^{n+1} = \frac{2}{\Delta t_c} \int_{t^n}^{t^{n+1}} P(t)dt - P_S^n$ :

$$\delta E_S = O(h^4) \tag{13}$$

Using a first order predictor (which means $\alpha_0 = 1$ and $\alpha_1 = 0$) and noticing that in this case $k_e < 0$, the first and third choice of $P_S^{n+1}$are attended to produce energy at the third order, which is sufficient with regard to the accuracy of the fluid and structural solvers. On the other hand, the second choice of $P_S^{n+1}$ will create energy at the first order, which must be seen in our simulations as a linear growth of the oscillations's amplitudes

### 3.4 Numerical Results

The structure is modeled in two dimensions for this test case, the spring being represented in MARC by a bloc of material of Young's Modulus $E_M$. It has a section $S_{M0} = S_0$ and an unstretched lenght of $L_{M0}$. Assuming that the poisson coefficient is set to zero, and that the displacements are small, this is equivalent to a spring of rigidity $k = \frac{E_M * S_0}{L_{M0}}$. Considering the 0D assumption, AVBP is replaced in the coupled software assembly by a simple 0D program which uses the information from MARC to compute $P_S^{n+1}$ according to Laplace's law. Figure(2) shows that the three choices of $P_S^{n+1}$ give a good agreement with theoretical results, the piston vibrating at the predicted frequency. In the same way figure(3), shows that the first and third choices of $P_S^{n+1}$ seem to well conserve the energy of the system, whereas as predicted previously, the second choice leads to a linear growth of the amplitude, thus of the energy.

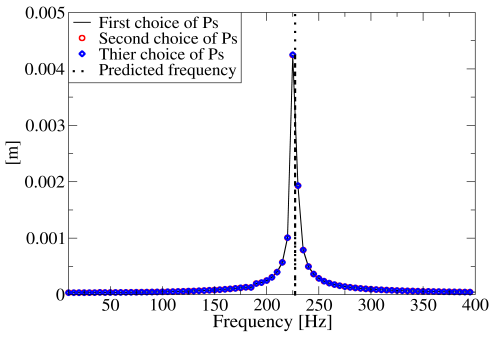


FIGURE 2 – Fourrier's Transform of the displacement

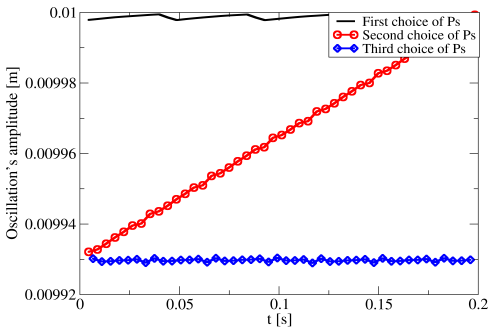


FIGURE 3 – Displacement's amplitude

# 4 Acoustic test configuration

This one dimensional test case is designed in order to account for the acoustics in a fluid-solid coupled system. Starting from rest, the fluid part will be disturbed with a pressure Dirac impulsion. After some iterations, coupled eigenfrequencies should appear while looking at the pressure signal in the chamber.

## 4.1 Device description

The set-up is composed of an adiabatic chamber filled with gas, closed at its left by a fixed wall and at the right by a deformable block of rubber fixed on its right side, see figure (4). The fluid chamber has a section $S_0$ and length $l_0$ when the block of rubber is at rest at $x = l_0$. The rubber of density $\rho_S$, has a Young modulus $E$ and a Poisson ratio $\nu$, and is fixed at $x = L_0$. Displacement (or position, depending the contest), velocity, and acceleration of a point $\vec{U}$ of the solid at time $t$ are respectively $\vec{U(t)}$, $\dot{\vec{U}}(t)$, and $\ddot{\vec{U}}(t)$.

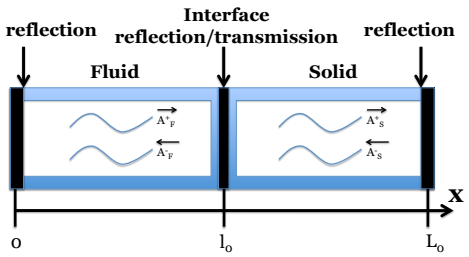


FIGURE 4 – Acoustic coupling system

The following assumptions are first made for the system :

- The gas is perfect with an adiabatic coefficient $\gamma$
- There is no external volume forces nor on the solid, neither on the fluid
- Both fluid and solid are considered with no dissipation
- The deformations of the solid are small, which allows to approximate the interface location by $l_0$

## 4.2 Acoustic Modelisation

Considering an eigen circular frequency $\omega_c$ of the coupled system, we have :

For the Fluid :
$$C_G = \sqrt{\gamma RT} \text{ and } k_G = \frac{\omega_c}{C_G}$$

For the Solid :
$$C_S = \sqrt{\frac{(1-\nu)E}{\rho_S(1+\nu)(1-2\nu)}} \text{ and } k_S = \frac{\omega_c}{C_S}$$

The reader can find a general method to evaluate the speed of sound in a solid in [1]. $P$ being the oscillating pressure and $\dot{U}$ the oscillating velocity, the wave propagation for both fluid and solid, can be written :

$$P_{G,S} = A^+_{G,S} e^{jk_{G,S}x} + A^-_{G,S} e^{-jk_{G,S}x} \tag{14}$$

$$\dot{U}_{G,S} = \frac{1}{\rho_{G,S} C_{G,S}} (A^+_{G,S} e^{jk_{G,S}x} - A^-_{G,S} e^{-jk_{G,S}x}) \tag{15}$$

Using (14) and (15) with the boundary conditions which are :

- $\dot{U}_G(0) = \dot{U}_S(0) = 0$ (wall no-slip condition for the fluid and embedding for the solid)
- $\dot{U}_G(l) = \dot{U}_S(l)$ (velocity continuity at the fluid structure interface located at $l_0$)
- $P_G(l) = P_S(l)$ (Stress continuity at the fluid structure interface located at $l_0$)

one can find that $\omega_c$ has to be the solution of (16) which can be solved numerically.

$$\frac{tan(\frac{\omega_c}{C_S}(l_0 - L_0))}{tan(\frac{\omega_c}{C_G}(l_0))} = \frac{\rho_S C_S}{\rho_G C_G} \tag{16}$$

### 4.3 Numerical Results

Both fluid and structure are modeled in two dimensions for this test case. In order to avoid any acoustic interference, a symmetry boundary condition has been used for the fixed bottom and top walls. This trick still ensures the absence of flow and thermal flux normal to the walls, and suppresses the impact of a noslip condition on the one dimensional assumption.
The solid is modelled in MARC by a bloc of material of Young's Modulus $E = 4.274\ 10^5\ Pa$ and Poisson's coefficient $\nu = 0$. It has a section $S_{M0} = S_0$ and an unstretched length of $L_{M0}$ . The calculation with the first and second choice of $P_S^{n+1}$ have been achieved using coupling time step ten times bigger than the fluid one (ie $\Delta t_{coupling} = \Delta t_{MARC} = 10\Delta t_{AVBP}$), and frequencies results are represented on figure(5). Unfortunately the third choice for $P_S^{n+1}$ appeared to be quickly numerically unstable. We don't have any valuable explanation to this behavior for the moment.

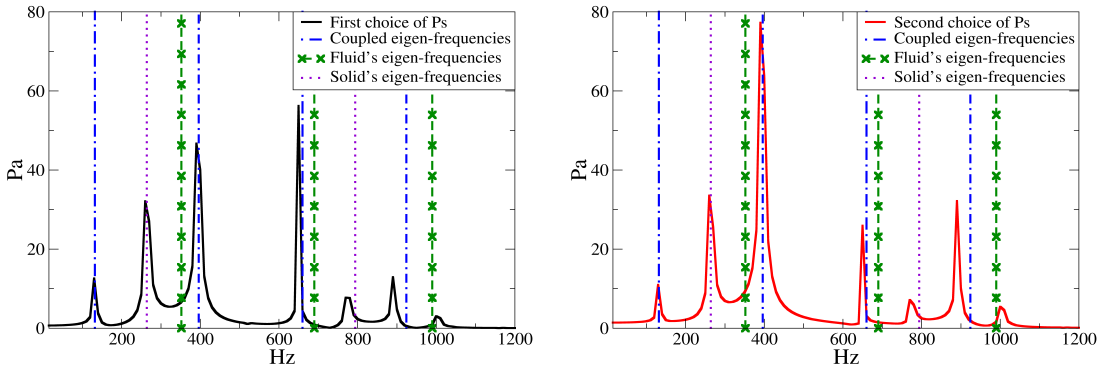


FIGURE 5 – Fourrier's Transform of the pressure at the middle of the chamber for the first choice of $P_S^{n+1}$ on the left hand side and for for the second choice on the right hand side

It's worth to notice on Fig.(5) that each choice of $P_S^{n+1}$ presents a good capacity to retrieve the coupling eigen frequency of the system. Nevertheless, looking at the spectra of the second choice of $P_S^{n+1}$ (ie $P_S^{n+1} = \frac{1}{\Delta t_c}\int_{t^n}^{t^{n+1}} P(t)dt$), one can notice that some modes are damped while others seem to be fed in comparison with the spectra obtained with $P_S^{n+1} = P^{n+1}$. This results is explainable with the same energy consideration than in the 0D part. Indeed, writing pressure and displacement at the fluid structure interface for one of the coupled eigen-modes leads to (17) which shows that the pressure and the structure are vibrating at the same circular frequency $\omega_c$ but with a phase depending of $k_G$ and $l_0$. The reader can check that the phase $\phi$ is $\pi$ if $\frac{1}{2}\sin(\frac{4\pi f_c l_0}{C_G}) > 0$ where $f_c$ is en eigenfrequency of the coupled system, and $\phi = 0$ in other cases. Using the same scalar $k_e$ and $h$ as in the 0D part, it comes out that the second choice of $P_S^{n+1}$ will feed in energy some modes and damp the others. This can be visualized on Fig.(6).

$$\begin{cases} U_G(l_0,t) = \dfrac{-2A_G^+}{\rho_G C_G \omega_c}\sin(k_G l_0)e^{-j\omega_c t} \\ P_G(l_0,t) = 2A_G^+\cos(k_G l_0)e^{-j\omega_c t} \end{cases} \tag{17}$$

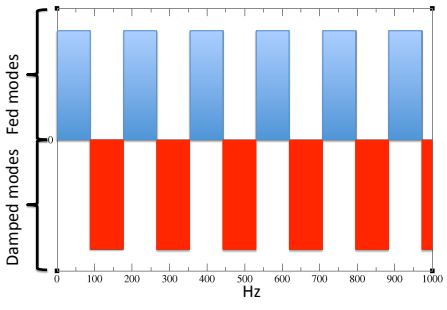


FIGURE 6 – Feeded and Damped modes

# 5 Conclusion

As predicted in the literature, it follows from these two test cases that the choice of $P_S^{n+1}$ is an important factor of the CSS method. As expected analytically, the first choice has shown a good energy conservation and a good behavior when dealing with acoustics. That is the reason why it appears to be adapted for our next applications. Indeed, including the fluid-structure interaction in solid propulsion simulation implies to be able to deal correctly with self-exited acoustic modes (see figure(8)) rising from a coupling between the hydrodynamics and the acoustic eigenmodes of the propellant's chamber (see figure(7) and figure(9)). The second choice must be avoided due to its poor energy conservation and it has shown unphysical feeding or damping for some modes. The third one gives good results in 0D, but it has shown itself numerically unstable in the 1D case.

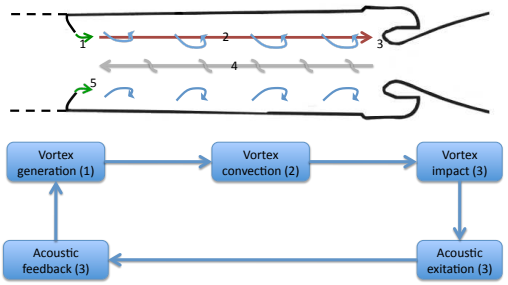


FIGURE 7 – Instabilities mechanism

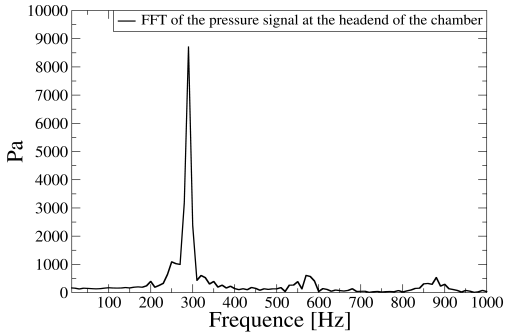


FIGURE 8 – Example of self-exited frequencies in a solid rocket motor


FIGURE 9 – Example of propellant's chamber

## Références


[1] C. Bacon, and J. Pouyet, *Mécanique Des Solides Déformables*, Hermes Science Publications (2000)

[2] S. Buis, A. Piacentini and D. Déclat, *PALM : A Computational Framework for assembling High Performance Computing Applications*,Concurrency and Computation, Vol. 18, N. 2, pp. 231-245 (2005)

[3] F. E. C. Culick, *Remarks on Acoustic Oscillations in a Solid Propellant Rocket*, AIAA J.Vol. 4 N. 6, pp. 1120-1121 (1966)

[4] P. Della Pieta, F. Godfroy, and J.-F. Guery, *Couplage Fluide/Structure applique en propulsion spatiale*, XVeme Congres Francais de Mecanique (2001)

[5] Y. Fabignon, J. Dupays, G. Avalon, F. Vuillot, N. Lupoglazoff, G. Casalis, M. Prévost. *Instabilities and pressure oscillations in solid rocket motors*, Aerospace Science and Technology, Vol. 7, N.3, pp. 191-200, (2003).

[6] C. Farhat and M. Lesoinne., *On the Accuracy, Stability, and Performance of the Solution of Three-Dimensional Nonlinear Transient Aeroelastic Problems by Partitioned Procedures*, AIAA paper 96-1388, In 37th AIAA/ASME/ASCE/AHS/ASC Structures, Structural Dynamics and Materials Conference, Salt lake City, Utah, April 18-19 1996

[7] J. Giordano, G. Jourdan, Y. Burtschell, M. Medale, DE Zeitoun, and L. Houas, *Shock wave impacts on deforming panel, an application of fluid-structure interaction*,Shock Waves, Vol.14 N.1, pp. 103-110 (2005)

[8] T.J. Huges, *The Finite element method. Linear static and dynamic finite element analysis*, Dover Publications New York (2000)

[9] E. Lefrançois, and J.P. Boufflet, *An Introduction to Fluid-Structure Interaction : Application to the Piston Problem*, SIAM review,Vol. 52 pp. 747 (2010)

[10] M. Lesoinne and C. Fahrat, *Stability Analysis of Dynamic Meshes for Transient Aeroelastic Computations* , AIAA paper 93-3325, In 11th AIAA Computational Fluid Dynamics Conference, Orlando, Florida, July 6-9 (1993)

[11] M. Lesoinne and C. Fahrat, *Geometric conservation laws for flow problems with moving boundaries and deformable meshes, and their impact on aeroelastic computations*, Computer methods in applied mechanics and engineering, Vol. 134 N. 1-2, pp. 71-90 (1996)

[12] F. Nicoud and F. Ducros, *Subgrid-scale stress modelling based on the square of the velocity gradient tensor*, *Flow, Turb. and Combustion* Vol. **62**, pp. 183-200 (1999)

[13] S. Piperno, C. Farhat, and B. Larrouturou, *Partitioned procedures for the transient solution of coupled aroelastic problems Part I : Model problem, theory and two-dimensional application*,Computer methods in applied mechanics and engineering, Vol. 124 N. 1-2, pp. 79-112 (1995)

[14] S. Piperno, and C. Farhat, *Partitioned procedures for the transient solution of coupled aeroelastic problems-Part II : Energy transfer analysis and three-dimensional applications*,Computer methods in applied mechanics and engineering, Vol. 190 N. 24-25, pp. 3147-3170 (2001)

[15] D. Ribereau, J.-F. Guery, and P. Le Breton, *Numerical Simulation of Thrust Oscillations of Ariane 5 Solid Rocket Boosters*, Space Solid Propulsion(2000)

[16] P. Schmitt, T. Poinsot, B. Schuermans, and K. P Geigle, *Large-eddy simulation and experimental study of heat transfer, nitric oxide emissions and combustion instability in a swirled turbulent high-pressure burner*, JFM Vol.570, pp.17-46 (2007)

[17] Schönfeld and M. Rudgyard, *Steady and unsteady flows simulations using the hybrid flow solver AVBP*, AIAA J., Vol. 37, N.11, pp. 1378-1385 (1999)

[18] M. A. F. Varela, *Modèles simplifiés d'interaction Fluide-Structure*, Université Paris IX Dauphine, (200)

[19] B. Wasistho, R. Fiedler, A.Namazifard and C. Mclay, *Numerical Study of Turbulent Flow in SRM with Protruding Inhibitors*, 42nd AIAA/ASME/SAE/ASEE Joint Propulsion Conference & Exhibit (2006)

[20] http ://www.mscsoftware.com/products/cae-tools/marc-and-mentat.aspx

[21] CERFACS. *AVBP Handbook*, http ://www.cerfacs.fr/4-26334-The-AVBP-code.php, 2009.